

# Signal and Power Integrity Co-Simulation for Multi-layered System on Package Modules

Krishna Bharath\*, Ege Engin\*, Madhavan Swaminathan\*, Kazuhide Uriu<sup>†</sup> and Toru Yamada<sup>†</sup>

\*School of Electrical and Computer Engineering

Georgia Institute of Technology, Atlanta, Georgia 30332-0250

Email: {kbharath, engin, madhavan.swaminathan}@ece.gatech.edu

<sup>†</sup>EMC Design Group, System Engineering Center

Matsushita Electric Industrial Co., Ltd.

Email: {uriu.kazuhide, yamada.-toru}@jp.panasonic.com

**Abstract**—The coupling of simultaneous switching noise (SSN) in mixed signal system on package modules is a critical signal and power integrity (SI/PI) problem. In the presence of split planes and apertures, SSN coupling occurs both horizontally as well as vertically across layers. Thus, to catch SI and PI problems at an early stage of design requires fast signal and power co-simulation methodologies. In this paper, we outline the multi-layer finite difference method and how the accuracy of the technique can be enhanced with models for fringe and gap effects. We then briefly describe a method for integrating the signal distribution network with the power distribution network to enable co-simulation. The method is then applied to a mixed signal board containing split planes, and numerical results are compared to full-wave simulations.

## I. INTRODUCTION

A high performance mixed signal system on package (SoP) module delivers power to its various components using power/ground planes. To reduce the parasitics of the power supply, as well as to increase high frequency decoupling, several power/ground planes can be arranged in an alternating manner. Signal lines are typically routed between these plane pairs.

Figure 1 shows a three layer package power distribution network (PDN) PDN supplying power to a mixed-signal IC. Multiple power supplies are typically required in modern SoPs due to the various integrated components. Split planes are required to provide DC isolation to the different supply voltages. Also, holes are created in the solid power/ground planes in order to route signals or to provide via anti-pads. The switching activity of digital circuitry causes a time varying current to be drawn from its power supply terminals, Vdd1-Gnd1. Due to the associated inductance of the loop, SSN is generated. SSN can couple horizontally across a plane pair and across power islands. Also, SSN couples vertically through vias, and through apertures. This can be regarded as a coupling by means of a wrap-around current on the edges of the planes. Through these mechanisms, ground bounce can occur across the Vdd2-Gnd2 planes.

In packaged mixed-signal SoP-based systems, there are multiple dissimilar modules in close proximity. In such systems, SSN can cause degradation of the performance of noise-sensitive RF components such as low noise amplifiers. Relatively low levels of coupled noise ( $\sim -60$  dB insertion loss between digital and RF modules) can cause significant performance degradation. Thus, it becomes critical to model split planes and apertures.

Another issue that arises due to the presence of split planes is that to facilitate communication between modules, signal lines might have to be routed over a slot. This causes a disruption in the return current path, which leads to the degradation of signal integrity. One reason that signal nets are routed between power/ground planes is that when these planes are solid, they can isolate adjacent signal layers. However, when apertures are created, this assumption is no

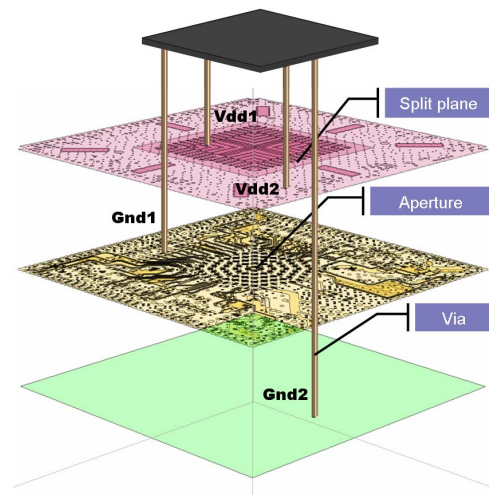


Fig. 1. SSN coupling mechanisms in a realistic package.

longer valid. Thus it becomes critical to co-simulate the signal and power distribution networks. While full-wave EM simulators are the most accurate tools to perform these simulations, the high time and memory complexity involved relegates the use of these tools to final verification.

A system-level SI/PI co-simulation methodology was proposed in [10]. A microstrip or stripline mode can be decoupled from the parallel plate mode using modal decomposition. The signal distribution network (SDN) and PDN can be analyzed separately and the results can then be reintegrated [4].

In [1], split planes have been modeled by employing lumped coupling elements. The values for these elements can be derived from closed form expressions based on the geometry of the problem. For narrow apertures, a transmission-line based model has been proposed to take into account interlayer coupling [8]. Electric and magnetic polarization currents have also been considered to compute coupling through electrically small cut-outs [9]. Recently, the multi-layer finite difference method (M-FDM) has been proposed in [5][3]. To the best of the authors' knowledge, M-FDM is the only efficient method available to analyze such structures with *arbitrarily large* holes in the planes.

The rest of the paper is organized as follows. The finite difference formulation for single plane pair geometries will be discussed in section 2, and its extension to multiple plane pairs (M-FDM) will be described in section 3. Addition of fringe and gap effects will be presented in section 4. The integration of the SDN and the PDN



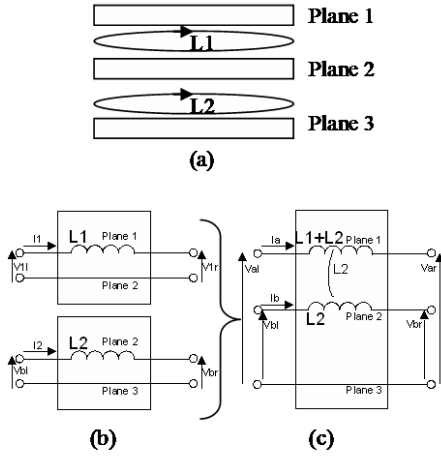


Fig. 3. (a) Side view of a unit cell for a 3 plane structure showing the current loops associated with the p.u.c. inductances. (b) P.u.c. inductance of each plane pair. (c) Combining the p.u.c. inductances by changing the reference planes.

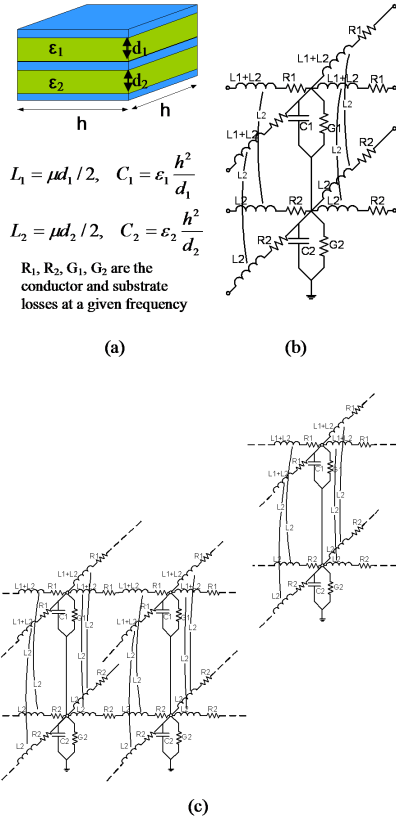


Fig. 4. (a) Geometry and p.u.c. parameters. (b) Combined unit cell model for three planes. (c) Plane model consisting of multilayer unit cells .

in [5], the total unit cell can be obtained as shown in Figure 4(b) for the example of three planes, where the bottom plane is chosen as the voltage reference plane. The equivalent circuit that would be obtained for a three layer geometry is shown in Figure 4(c).

For solid multilayered rectangular planes, discretized with  $M_1$  cells in the  $x$ -direction and with  $M_2$  cells in the  $y$ -direction, the admittance matrix  $\bar{\bar{Y}}$  can be written as

$$\bar{\bar{Y}} = \begin{pmatrix} \bar{\bar{A}} & \bar{\bar{B}} & & & \\ \bar{\bar{B}} & \bar{\bar{A}} - \bar{\bar{B}} & \bar{\bar{B}} & & \\ & \bar{\bar{B}} & \ddots & \ddots & \\ & & & \ddots & \bar{\bar{B}} \\ & & & & \bar{\bar{A}} \end{pmatrix} \quad (6)$$

where  $\bar{\bar{A}} =$

$$\begin{pmatrix} \bar{Y}_{uc} + 2\bar{Z}_{uc}^{-1} & -\bar{Z}_{uc}^{-1} & & & \\ -\bar{Z}_{uc}^{-1} & \bar{Y}_{uc} + 3\bar{Z}_{uc}^{-1} & -\bar{Z}_{uc}^{-1} & & \\ & -\bar{Z}_{uc}^{-1} & \bar{Y}_{uc} + 3\bar{Z}_{uc}^{-1} & \ddots & \\ & & \ddots & \ddots & -\bar{Z}_{uc}^{-1} \\ -\bar{Z}_{uc}^{-1} & \bar{Y}_{uc} + 3\bar{Z}_{uc}^{-1} & -\bar{Z}_{uc}^{-1} & & -\bar{Z}_{uc}^{-1} \\ & & & -\bar{Z}_{uc}^{-1} & \bar{Y}_{uc} + 2\bar{Z}_{uc}^{-1} \end{pmatrix} \quad (7)$$

and

$$\bar{\bar{B}} = \begin{pmatrix} -\bar{Z}_{uc}^{-1} & & & \\ & \ddots & & \\ & & & -\bar{Z}_{uc}^{-1} \end{pmatrix} \quad (8)$$

Here,  $\bar{\bar{A}}$  and  $\bar{\bar{B}}$  are  $kM_1 \times kM_1$  matrices for  $(k+1)$  planes, assuming that the nodes are numbered starting from the top node in the lowest row, increasing in the vertical direction to the bottom node, then starting with the next cell in the  $x$ -direction until the last cell, and then starting with the next row. Hence,  $\bar{\bar{Y}}$  is a  $(kM_1 M_2) \times (kM_1 M_2)$  matrix. The unit cell matrices,  $\bar{Y}_{uc}$  and  $\bar{Z}_{uc}^{-1}$  are tri-diagonal and are given by

$$\bar{Y}_{uc} = \begin{pmatrix} Y_1 & -Y_1 & & & \\ -Y_1 & Y_1 + Y_2 & -Y_2 & & \\ & -Y_2 & \ddots & \ddots & \\ & & & -Y_{k-2} & -Y_{k-1} \\ & & & -Y_{k-2} & Y_{k-2} + Y_{k-1} & -Y_{k-1} \\ & & & & -Y_{k-1} & Y_{k-1} + Y_k \end{pmatrix} \quad (9)$$

and

$$\bar{Z}_{uc}^{-1} = \begin{pmatrix} -\frac{1}{Z_1} & \frac{1}{Z_1} & & & \\ \frac{1}{Z_1} & -\frac{1}{Z_1} & \frac{1}{Z_2} & & \\ & -\frac{1}{Z_2} & \ddots & \ddots & \\ & & & -\frac{1}{Z_{k-2}} & \frac{1}{Z_{k-2}} \\ -\frac{1}{Z_{k-2}} & \frac{1}{Z_{k-2}} & \frac{1}{Z_{k-1}} & & \\ & & -\frac{1}{Z_{k-1}} & \frac{1}{Z_{k-1}} & \frac{1}{Z_k} \end{pmatrix} \quad (10)$$

where  $Y_i$  and  $Z_i$  can be obtained similar to the unit cell parameters for a single plane pair structure as

$$Y_i = j\omega C_i + \omega C_i \tan \delta_i \quad (11)$$

$$Z_i = 2j\omega L_i + \frac{2}{\sigma t} + 2\sqrt{\frac{j\omega\mu}{\sigma}} \quad (12)$$

By an analysis similar to what was provided in the previous section, it can be shown that the computational complexity of M-FDM applied

to  $k + 1$  layers is  $O(N^2)$  where  $N = (kM_1M_2)$ . Typically in the presence of mutual inductor elements such as what has been shown in Figure 4, the unit cell inductance matrix  $\bar{Z}_{uc}^{-1}$  will be full-dense. However, the nature of the loop inductances considered lends to the tri-diagonal form shown in (10) and hence to the unique advantages of M-FDM.

#### IV. INCLUSION OF SECONDARY EFFECTS

##### A. Fringe Effect Models

The M-FDM formulation discussed in the previous sections assumes that each unit cell sees plane-pairs of infinite extent along the lateral directions. However, fringing fields occur at edge discontinuities. This implies that both the per-unit-length (p.u.l) inductance and capacitance will be different from that obtained from parallel plate formulae. This problem has been considered in [7], which proposes building a library that maps various geometries to model elements, and interpolating between these values. However, this technique requires the development of a large database that accounts for variations in dielectric height and permittivity, trace width and metal height, and can suffer from interpolation errors. On the other hand, the technique proposed in [1] relies on well characterized closed form expressions which are easy to implement. The fringe fields are

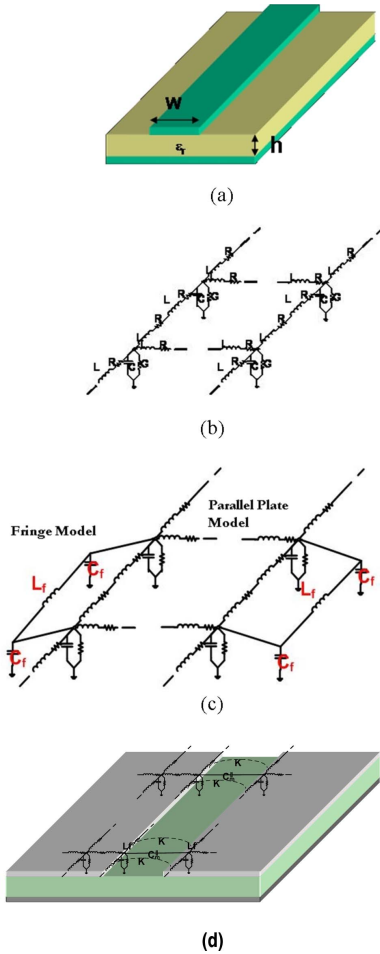


Fig. 5. (a)Geometry (b)Representation with the FDFD model (c)Correction for fringe effect by addition of elements  $C_f$  and  $L_f$ (d)Gap model with addition of gap elements,  $C_m$  and  $K$ .

corrected by adding additional elements to edges. A microstrip line

of width  $W$ , dielectric height  $h$  and metal thickness  $t$  is shown in Figure 5(a). The M-FDM model for this microstrip is shown in Figure 5(b). The fringe effect is modeled by the addition of  $L_f$  and  $C_f$ , as shown in Figure 5(c), and are given by [1]

$$C_f = \frac{C_{pul} - C_{pp}}{2} w \quad (13)$$

$$L_f = \frac{2\mu h w L_{pul}}{\mu h - W L_{pul}} \quad (14)$$

where,  $C_{pul}$  and  $L_{pul}$  are the p.u.l capacitance and inductance of a microstrip line of equivalent width, dielectric height  $h$  and permeability  $\mu$ .  $C_{pp}$  is the p.u.l parallel plate capacitance and  $w$  is the unit cell width.

##### B. Gap Effect Models

Coupling occurs between physically separated metal patches when the distance of separation between them approaches the dielectric thickness. The coupling can be especially significant when the patches resonate. Figure 5 shows split planes of width  $W$  separated by a spacing  $s$ , with a dielectric height  $h$ . The gap is modeled by considering both the  $E$ -field and  $H$ -field coupling. The  $E$ -field coupling is represented by a capacitor,  $C_m$ , connected between the nodes that lie across the gap. The  $H$ -field coupling is modeled by a mutual coupling factor,  $K$ , as shown in Figure 5. The values of  $C_m$  and  $K$  are obtained by applying coupled line theory as explained in [1].

The addition of the fringe models do not increase the complexity of the problem as they represent only a correction to existing circuit elements. However, the addition of the gap elements will increase the bandwidth of the admittance matrix, as the width of a split plane may be discretized by more than one unit cell. However, it is known that coupling between patches becomes less significant as the ratio of the gap spacing  $s$  to the dielectric height  $h$  becomes large, for which the gap model may not be applied. This allows the computational complexity of the proposed approach to be maintained at  $O(N^2)$ .

#### V. INTEGRATION OF THE SDN AND THE PDN

Since separate analyses of the SDN and the PDN fails to account for the coupling between the two domains, the two responses need to be integrated to perform an accurate system level analysis. This integration can be performed using the admittance matrices of the two modules along with the stamp rule [2]. The process involves conversion of the SDN response into its equivalent model which is then stamped onto the admittance matrix of the PDN. This ensures that all parasitic effects between the PDN and the SDN are accurately accounted for in the integration process.

For example in a simple microstrip interconnect referenced to non-ideal power ground planes, since the transmission line and parallel-plate modes are not coupled, the integration of the SDN and the PDN responses can be carried out simply by combining the two Y-matrices as given by

$$\begin{pmatrix} I_p^i \\ I_p^o \\ I_m^i \\ I_m^o \end{pmatrix} = \begin{pmatrix} Y_p & 0 \\ 0 & Y_m \end{pmatrix} \begin{pmatrix} V_p^i \\ V_p^o \\ V_m^i \\ V_m^o \end{pmatrix} \quad (15)$$

where  $Y_p$  and  $Y_m$  are the Y-matrices of the power/ground planes and the microstrip interconnect (considering ideal reference) respectively, while  $I$  and  $V$  are the vectors defining the currents and the voltages at the input and output ports. However, if the current on the signal line excites both modes, like in the case of a stripline interconnect referenced to non-ideal power/ground planes, additional considerations



[3] are required to integrate the SDN and the PDN responses. For the stripline case, the SDN and the PDN responses can be integrated as given by

$$\begin{pmatrix} I_p^i \\ I_p^o \\ I_m^i \\ I_m^o \end{pmatrix} = \begin{pmatrix} k^2 Y_s + Y_p & k Y_s \\ k Y_s & Y_s \end{pmatrix} \begin{pmatrix} V_p^i \\ V_p^o \\ V_m^i \\ V_m^o \end{pmatrix} \quad (16)$$

where  $Y_p$  and  $Y_s$  are the Y matrices of the power/ground planes and the stripline (considering ideal reference) respectively, and  $k$  is a constant determined from the layout. Once the integration is complete, the line terminations and the other lumped components in the system can be added to the overall system matrix using the stamp rule. Since the transient response is often required only at particular locations in the system, the overall system matrix can be reduced to include ports only at those locations where the system is being excited or probed. The reduced system matrix thus obtained is then used for estimating the port-to-port delays in the system to enforce causality on the transient response.

## VI. RESULTS

The methodology described in prior sections has been implemented in a CAD tool. Simulations were performed to compare the methodology against full-wave simulations and measurements, and to demonstrate the scalability of the method. All simulations were performed on an Intel Xeon workstation with a 3.2 GHz processor and 3.5 GB of RAM. Full-wave simulations were performed with the method-of-moments based solver, Sonnet.

A mixed signal board of size 60mm  $\times$  34.8 mm is shown in Figure 6(a). A microstrip transmission line originates from an FPGA located near port 1, and connects to a low noise amplifier (LNA) at port 2. The microstrip, which is of length 34 mm, traverses over the slot separating the power islands of the two modules. The dielectric height between the power/ground planes was 300  $\mu\text{m}$ , and between the signal and power planes is 200  $\mu\text{m}$ . The dielectric was FR-4 with  $\epsilon_r = 4.4$ .

This example was simulated in Sonnet as well as M-FDM using a cell size of 0.3mm. In M-FDM, the PDN was simulated first. The transmission line was broken into three segments, with the first and last segment represented by a microstrip referenced to the power layer. The middle segment represents the section of the microstrip that is present above the slot and is hence reference to the ground layer. The results obtained from simulation are shown in Figures 6(b) - (e). Figures 6(b) and (c) show the case when the microstrip is assumed to be ideal. In this case, there are no discontinuities, and since the characteristic impedance is  $\sim 54\Omega$ , the dB( $S_{12}$ ) is very close to zero. However, when the microstrip is routed over the slot, the obtained return and insertion loss results are shown in Figures 6(d) and (e). In this case, the insertion loss is significantly higher.

As can be seen from the return loss and the insertion loss results, we are able to get good correlation between Sonnet and M-FDM. The Sonnet simulations required 800s per frequency point analyzed, while in M-FDM required 3.2s per frequency point. This represents a speedup of about 200X. A 0.4 mm wide microstrip line traversing a 2.5 mm slot in the power plane is shown in Figure 7. The transmission line in this case is assumed to be an interconnect driven by a 533 MHz DDR II driver. In this case each power island is of size 125 mm  $\times$  100 mm. The dielectric height between the microstrip line and the power plane is 0.2 mm. The dielectric height between the power and ground planes is 1 mm. A simple rectangular geometry is chosen

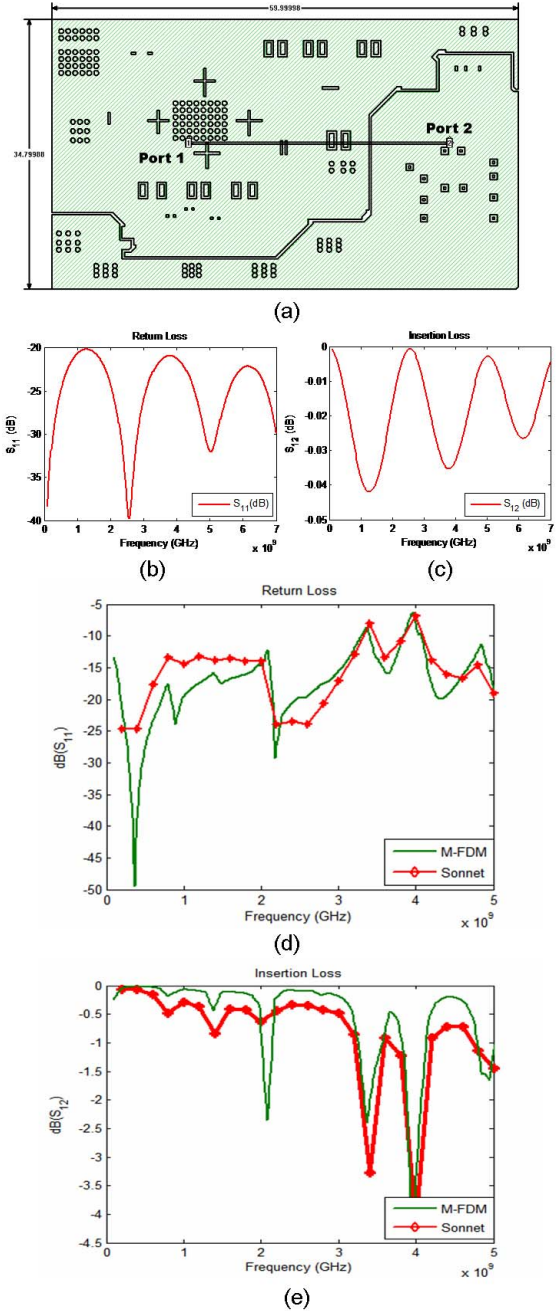


Fig. 6. (a) Mixed signal board with transmission line traversing a slot (b) Return loss results - Ideal Microstrip (c) Insertion loss results - Ideal Microstrip (d) Return loss results (e) Insertion loss results.

since it is possible to analytically compute the resonant frequencies using the formula

$$f_{cm,n} = \frac{1}{2\pi\sqrt{\mu\epsilon}} \sqrt{\left(\frac{m\pi}{a}\right)^2 + \left(\frac{n\pi}{b}\right)^2} \quad (17)$$

where  $a$  and  $b$  represent the length and width of the rectangular geometry. Given a dielectric constant,  $\epsilon_r$ , of 4.4, the first resonance occurs at 570 MHz. Figure 8 shows the insertion loss of the transmission line. It can clearly be seen that the resonance of the planes gives rise to significant insertion loss (-8dB). A method that can be used

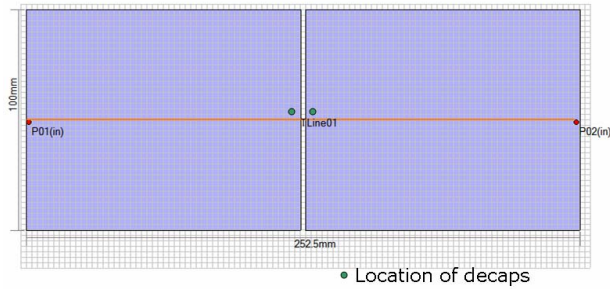


Fig. 7. Top view of test case. Microstrip interconnects ports 1 and 2.

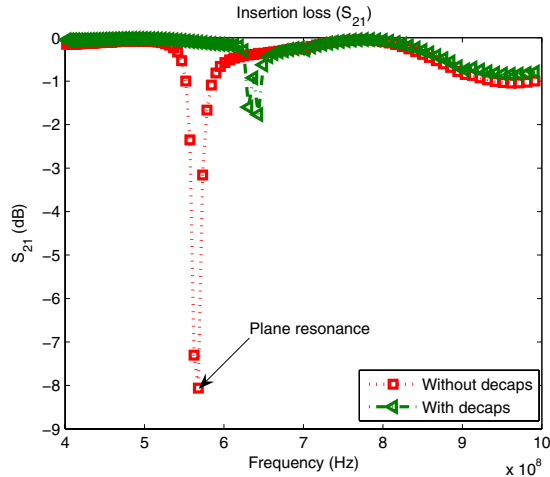


Fig. 8. Insertion loss results for structure in Figure 7.

to suppress this resonance is by using decoupling capacitors with a self resonant frequency of around 570 MHz. Two such capacitors are placed at locations close to the gap as shown in Figure 7. The parasitic series resistance of the capacitor was  $10\text{ m}\Omega$ , and its series inductance was around  $0.8\text{ nH}$ . It can be seen from Figure 8 that after placement of the decaps, the insertion loss is significantly improved. The simulation time per frequency point using M-FDM was 100 ms, demonstrating how the method can be employed to efficiently co-simulate SI/PI problems.

## VII. CONCLUSION

The ever increasing integration of package level integration has given rise to new SI and PI problems that cannot be solved at present with full-wave simulation tools. This has led to the need for efficient CAD tools. The multi-layer finite difference method has been proposed as an accurate and efficient simulation engine for power distribution networks. The accuracy of the method can be improved by the inclusion of circuit models for the fringe and gap effects. Modal decomposition techniques have been employed to integrate the SDN and PDN to enable SI/PI co-simulation. The proposed methodology has been applied successfully to a mixed-signal board with split planes.

## REFERENCES

[1] K. Bharath, E. Engin, M. Swaminathan, K. Uriu, and T. Yamada. Efficient modeling of package power delivery networks with fringing fields and gap coupling in mixed signal systems. In *Proc. of 15th IEEE EPEP*, pages 59–62, Oct. 2006.

[2] J. A. Dobrowolski. *Introduction to Computer Methods for Microwave Circuit Analysis and Design*. Artech House, 1991.

[3] A. E. Engin, K. Bharath, K. Srinivasan, and M. Swaminathan. Modeling of multilayered packages and boards using modal decomposition and finite difference methods. In *Proc. of 2006 IEEE EMC Symposium*, Aug. 2006.

[4] A. E. Engin, W. John, G. Sommer, and W. Mathis. Modeling of non-ideal planes in stripline structures. In *Proc. of 12th IEEE EPEP*, pages 247–250, Oct. 2003.

[5] E. Engin, K. Bharath, M. Swaminathan, and et. al. Finite-difference modeling of noise coupling between power/ground planes in multilayered packages and boards. In *Proc. of 56th ECTC*, pages 1262 – 1267, June 2006.

[6] A. George. Nested dissection of a regular finite element mesh. *SIAM Journal on Numerical Analysis*, 10(2):345–363, April 1973.

[7] C.-C. Huang and C. Luk. Accurate analysis of multi-layered signal and power distributions using the fringe rlgc models. In *Proc. of 13th IEEE EPEP*, pages 103–106, Oct. 2004.

[8] R. Ito and R. Jackson. Parallel plate slot coupler modeling using two dimensional frequency domain transmission line matrix method. In *Proc. of 13th IEEE EPEP*, pages 41–44, Oct. 2004.

[9] J. Lee, M. Rotaru, M. Iyer, H. Kim, and J. Kim. Analysis and suppression of ssn noise coupling between power/ground plane cavities through cutouts in multilayer packages and pcbs. *IEEE Trans. Adv. Packag.*, 28(2):298–309, May 2005.

[10] R. Mandrekar, K. Bharath, K. Srinivasan, E. Engin, and M. Swaminathan. System level signal and power integrity analysis methodology for system-in-package applications. In *Proc. of 43rd DAC*, pages 1009 – 1012, July 2006.

[11] E. T. Itoh. *Numerical Techniques for Microwave and Millimeter-Wave Passive Structures*. John Wiley, 1989.